USB Proceedings

2016 XXII International Conference on Electrical Machines (ICEM)

SwissTech Convention Center
Lausanne, Switzerland
04 - 07 September, 2016

Sponsored by

The International Conference of Electrical Machines Association (ICEM)
The Institution of Engineering and Technology (IET)
The IEEE Industrial Electronics Society (IEEE-IES)
The IEEE Industry Applications Society (IEEE-IAS)

IEEE Catalog Number: CFP1690B-USB
ISBN: 978-1-5090-2537-4

Cost-oriented design of high speed low power interior permanent magnet synchronous machines

Aryanti Kusuma Putri, Marco Hombitzer, David Franck and Kay Hameyer, *Senior Member, IEEE*

***Abstract*—In this paper, the characteristic of interior permanent magnet synchronous machine (IPMSM) with concentrated windings is evaluated for three different rotor geometries. The reference machine is a fractional horsepower IPMSM with single-layer magnets (1-layered IPMSM). The maximum output power of the machine is 820 W. Based on the electrical properties and machine cost of the reference machine, IPMSM with two different rotor geometries are designed. The first one is an IPMSM with v-shaped magnets (VPMSM) and the second is an IPMSM with double-layer magnets topology (2-layered IPMSM). The machines are compared in two operating points: one in the base speed area and one in the field weakening range. The focus of the machine comparison are the parasitic effects due to the non-sinusoidal rotor field, e.g. back-emf harmonics, torque harmonics, radial force densities and iron losses.**

Index Terms*—air gap flux densities, low power drives, low cost machines, permanent magnet synchronous machines, radial force densities, rotor pole shaping, torque harmonics

I. Introduction

The permanent magnet synchronous machines (PMSM) exhibit high power and torque density, when compared to other types of electrical machines. For this reason, PMSM are widely used in applications which have low space and light weight requirements. The torque of a PMSM can be decomposed in two components: the synchronous torque and the reluctance torque. The synchronous torque is generated by the interaction of stator and rotor fields. The reluctance torque is caused by the difference of the magnetic reluctance in direct and quadrature axes. Due to the homogeneous reluctance on both axes, a surface mounted synchronous machine (SPMSM) possesses only a synchronous torque. The interior permanent magnet synchronous machines (IPMSM) exhibit a lower synchronous torque when compared to SPMSM. This can be compensated with the reluctance torque of the machine. To achieve higher power densities, the use of high-speed machines are increased in the recent years. Due to the good flux weakening capability of IPMSM, this type of machine is more attractive for applications with a wide constant-power range when compared to SPMSM ([1], [2]).

The objective of this paper is to compare different types of IPMSM regarding its characteristic in different working areas: base speed area ($n_1 = 610\,\mathrm{min}^{-1} \& M_1 = 1.31\,\mathrm{Nm}$) and field weakening range ($n_2 = 19520\,\mathrm{min}^{-1} \& M_2 = 0.26\,\mathrm{Nm}$). The main issue of the machine design is the speed difference of both operating points, which ratio is $n_1 : n_2 = 1 : 32$. Furthermore, the available construction space of the machine is strongly limited. In Table I the geometrical and electrical requirements of the machine are listed.

A. K. Putri, M. Hombitzer, D. Franck and K. Hameyer are with Institute of Electrical Machines, RWTH Aachen University, Aachen, Germany (e-mail: aryanti.putri@iem.rwth-aachen.de).

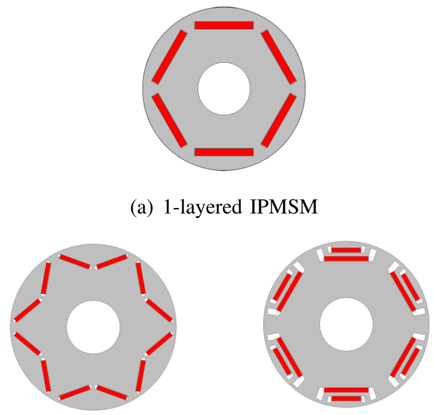

(a) 1-layered IPMSM

(b) VPMSM (c) 2-layered IPMSM

Fig. 1: The basic geometry of the examined rotors.

Three different rotor geometries are studied and examined concerning the parasitic effects in the chosen working points, e.g back-emf harmonics, torque harmonics, radial force densities and iron losses. The basic geometries of the rotors are shown in Fig. 1. The basic geometry represents the rotor geometry without modification on its surface (round rotor). In Fig. 1 (a) the basic geometry the reference machine, IPMSM with single layer magnets (1-layered IPMSM), is shown. To reduce the torque ripple and the back-emf harmonics the surface of the rotor is modified with methods introduced in [3] and [4]. In Fig. 1 (b) and Fig. 1 (c) the basic geometry of the alternative machines are drawn. These are IPMSM with v-shaped magnets (VPMSM) and IPMSM with double-layer magnets (2-layered IPMSM), which exhibit high ratio of reluctance to overall torque. Through utilization of the reluctance torque, alternative machines with lower cost and higher efficiency with equivalent machine qualities, such as the torque ripple and the acoustic radiation, are designed. The characteristic of the final machines will be evaluated and compared with the reference machine.

TABLE I: Geometrical and Electrical Requirements of the IPMSM.

Stator outer radius $r_{stator,o}$	60 mm
Minimum air gap length δ	0.7 mm
Axial length l_{Fe}	30 mm
Number of Poles / Slots $2p/N$	6 / 9
Magnet type	NdFeB
Minimum magnet height	2 mm
Winding type	single-tooth winding
Maximum input voltage U_{line}	190 V
Maximum phase current I_{eff}	7.1 A

978-1-5090-2537-4/16/$31.00 ©2016 IEEE

II. Simulation

By a Finite-Element-Modell (FE) the rotor angle dependent back-emf, torque and torque harmonics, radial force densities, and iron losses are simulated.

The back-emf of each phase are determined through differentiation of the phase magnetic flux for every rotor angle, which is calculated through surface integration of the flux density B for every element of each winding. In the next step, the resistance of each winding R_1 is considered by a multiplication with the phase current i_1. The line-to-line voltage u_{line} is calculated by subtraction of two phases. It can be described with the equations:

$$\begin{aligned} u_{phase,1}(t) &= -\frac{d}{dt}\iint B(t)\,dA + i_1(t)R_1 \\ u_{line,12}(t) &= u_{phase,1}(t) - u_{phase,2}(t). \end{aligned} \tag{1}$$

The torque and the torque harmonics are calculated with the methods introduced in [5], which is based on the eggshell method [6]. The sum of the forces F_k on every node k (nodal force) multiplied by its distance to the origin of the rotor r_k represent the torque T in one point in time:

$$T = \Sigma\, r_k \times F_k. \tag{2}$$

Employing (2) for multiple time steps for one rotation of the rotor, the mean torque and torque harmonics can be determined.

The radial force densities acting on the stator are evaluated through decomposition of the nodal forces in the tangential and radial components, which are normalized to the length of the machine. The radial force densities can be decomposed by 2D Fourier transformation in time and spatial orders. The sensitive hearing range of humans lies between 2-5 kHz [7]. To estimate the acoustic radiation of the machines, the occured low spatial orders within this frequency range with a deviation of 1 kHz are compared.

The iron losses are calculated by the IEM-Formula for electrical machines, which is described in [8] and [9]:

$$\begin{aligned} P_{v,Fe} &= a_1\,B^2\,f_{el.} \\ &+ a_2\,B^2\,f_{el.}^2(1 + a_3\,B^{a_4}) \\ &+ a_5\,B^{1.5}\,f_{el.}^{1.5}. \end{aligned} \tag{3}$$

$f_{el.}$ and a_1 to a_5 are electrical frequency and the iron loss parameters. The parameters are listed in Table II. These are derived from the manufacturer data and fitted according to the measurements in two working points of the reference machine. The iron losses are calculated for each element in every time step and the harmonics of flux density B are taken into account.

TABLE II: a-Parameters for Iron Loss Calculation.

a_1	$88.74 \cdot 10^{-3}$
a_2	$73.76 \cdot 10^{-6}$
a_3	$284.40 \cdot 10^{-3}$
a_4	3
a_5	0

III. Design

In this section the machine requirements and the design methods of the alternative machines are described. The stator geometry parameter, such as the height of the yoke and the width of the stator teeth, are kept constant. Hence, the acoustic radiation level can be estimated by the calculation of the radial force densities. The combination of the rotor poles and stator slots is not changed, so that the dominant temporal and spatial orders of the force excitations are preserved. To achieve lower cost, the magnet volume of the alternative machines shall not exceed the magnet volume of the reference machine.

A. Machine Requirements

The reference machine has two operating points: base speed area with speed $n_1 = 610\,\mathrm{rpm}$ and torque $M_1 = 1.31\,\mathrm{Nm}$ (OP 1) and field weakening range with speed $n_2 = 19520\,\mathrm{rpm}$ and torque $M_2 = 0.26\,\mathrm{Nm}$ (OP 2). The electrical operating points are defined by the control of maximum torque per ampere (MTPA) and maximum torque per voltage (MTPV), which are described in [10]. In Table III the simulation results of the relevant operating points are listed. These serve as design orientation of the alternative machines. The minimum efficiency in OP 1 and OP 2 are 62 % and 74 % at the winding temperatur of 70 °C respectively. Furthermore, the required maximum output power $P_{\max}$ is 820 W and the minimum output power between the speed $n = 5000 - 20000\,\mathrm{min}^{-1}$ is $P_{\min} = 700\,\mathrm{W}$. The rotor surface velocity at $n = 20000\,\mathrm{min}^{-1}$ is $60\,\mathrm{m/s}$. In Table IV the frequencies of the dominant temporal orders dependent on the operating points are listed. It can be concluded, that only the force excitations in OP 2 are relevant for the acoustic radiation.

From Table III can be concluded, that the copper losses are dominant in both operating points. To prevent the increase

TABLE III: Operating Points of the Reference Machine.

	OP 1	OP 2
Speed / rpm	610	19520
Torque / Nm	1.31	0.26
Output power / W	83.68	531.47
Copper losses / W	38.75	60.62
Iron losses / W	3.14	42.56
Efficiency / %	66.06	79.30
Torque ripple / Nm	0.03	0.01
Radial force density orders (temporal, spatial) / $\mathrm{kN/m^2}$		
(6, -3)	15.29	5.24
(6, 6)	8.76	2.11
(12, -6)	1.83	1.15
(12, 3)	0.74	1.06
(18, 0)	0.49	0.16
Magnet volume / $\mathrm{mm^3}$	8820	

TABLE IV: Frequencies of the Radial Force Densities.

	Frequency / Hz	
Temporal Order	OP 1	OP 2
6	61	1952
12	122	3904
18	183	5856

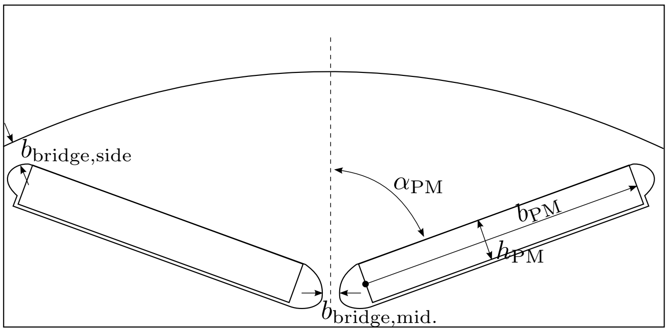

Fig. 2: Pole Geometry of a VPMSM.

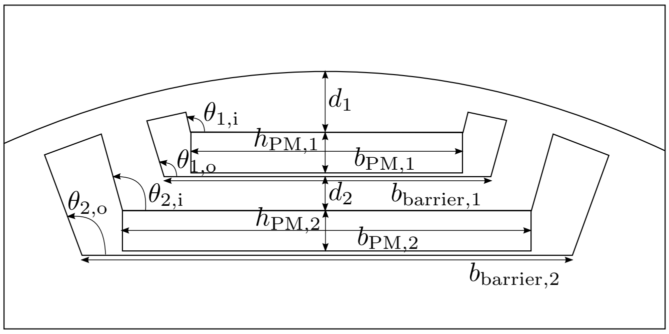

Fig. 3: Pole Geometry of an IPMSM.

of these losses, the minimum amplitude of the flux density fundamental harmonic of the alternative machines is set to the amplitude of the flux density fundamental harmonic of the reference machine, which is 0.6 T.

One of the main causes of the parasitic effects in electrical machines, such as torque ripple and acoustic radiation, is the flux density harmonics of the rotor. These effects can be reduced through minimizing the total harmonic distortion (THD) of the rotor flux density. The THD is calculated with the equation:

$$THD = \sqrt{\frac{\sum\limits_{\mu>1} {B^{\mu}_{rad}}^2}{\sum\limits_{\mu} {B^{\mu}_{rad}}^2}}\,. \tag{4}$$

To ensure the mechanical stability, the rotors are designed to have the maximum stress of 350 MPa at $n = 30000\,\mathrm{min}^{-1}$, which is 1.5 times the maximum speed of the machines. Due to the manufacturing limitation, minimum distance between the rotor bridges is set to 0.5 mm.

B. Design of the VPMSM

Due to the flux concentrating topology and high reluctance ratio L_q/L_d, VPMSM exhibits high synchronous and reluctance torque when compared to conventional 1-layered IPMSM with the same magnet mass [11]. The disadvantages of VPMSM to 1-layered IPMSM are for example the high cogging torque and torque ripple. To subdue this problem, the rotor alteration according to [12] will be applied on the rotor surface. With this measure, the cogging torque and torque ripple of the VPMSM can be reduced [13]. The disadvantage of this surface alteration method is the reduction of the reluctance ratio L_q/L_d and thus the reluctance torque [14].

In Fig. 2 a pole of a VPMSM and its geometric parameters are shown. The pole pitch factor $\tau_{\mathrm{M}}/\tau_{\mathrm{p}}$ is chosen to reach high effective torque and low torque ripple simultaneously. In the case of a VPMSM, the optimal value of the pole pitch factor lies between 0.7 - 0.8 [15]. To minimize the leakage flux, the side bridge and the middle bridge between the poles ($b_{\mathrm{bridge,side}}$ and $b_{\mathrm{bridge,mid.}}$ respectively) have to be kept thin. The first design step is the variation of the magnet angle α_{PM} at a constant pole pitch factor. The magnet height is kept at its minimum value. The width of the permanent magnet increases with smaller magnet angle, which leads to a larger area of the magnet's surface in the magnetization direction and increase of the synchronous torque. Due to less amount of electrical steel, the inductivity in the d-axis decreases with smaller magnet angle and thus, the reluctance torque increases. As a conclusion, the effective torque of the machine increases with smaller magnet angle.

Through minimizing the used amount of magnet materials, the overall cost can be reduced. Hence, the permanent magnet width is reduced until the minimum amplitude of the rotor flux density fundamental harmonic in the air gap is reached. In Fig. 2 the reduction of the permanent magnet width is illustrated through the arrow with a dot at its starting point. The position of the starting point is kept constant, only the length of the arrow is reduced. The amount of the magnet material is decreased without changing the reluctance of the machine. The last design step of the VPMSM is the rotor surface modification according to [12] to reduce the THD of the rotor flux density.

C. Design of the 2-layered IPMSM

The 2-layered IPMSM possesses in general low synchronous torque when compared to 1-layered IPMSM. However, the saliency of a 2-layered IPMSM is superior to a 1-layered IPMSM. This compensates the disadvantage regarding the synchronous torque. It is shown in [16], that a 2-layered IPMSM can reach higher efficiency than 1-layered IPMSM without additional increase of magnet material. To mantain the reluctance torque, measures to reduce parasitic effects through modification of the rotor's surface will not be taken. The measures to minimize the parasitic effects of a 2-layered IPMSM is studied in [17]. Through variation of the flux barrier angles, the torque ripple and the radial force excitation of a 2-layered IPMSM can be minimized.

In Fig. 3 a pole of a 2-layered IPMSM and its geometry parameters are shown. Theoretically, a small distance of the permanent magnets to the air gap is advantageous. The amplitude of the rotor flux density increases with smaller distance to the air gap. However, this is only a minor effect when compared to the permanent magnet width. It is advantageous to have larger distances d_1 and d_2 than smaller permanent magnet widths. Moreover, the distance between the air gap and the first magnet d_1 is required, so that the flux barrier angles of the first permanent magnet can be variated without limitation. The barrier width b_{barrier} affects the form of the air gap flux density, particularly the first slope after the intersection of the poles. An approximation of a sinusoidal air gap flux density can be attained by the design of the barrier width. This effect can also be achieved through variation of the flux barrier angles of the second permanent magnet.

The 2-layered IPMSM will be designed based on the sum of the magnet material of the VPMSM with rotor surface modification. The first step is to choose the ratio $b_{\mathrm{PM},1}/b_{\mathrm{PM},2}$. The height of both magnets is kept at its minimum value. The objective is to design a rotor that induces high air gap flux density with sufficiently low THD. The position of the magnets are changed dependent on the magnet width.

After choosing the suitable magnet ratio, the flux barrier angles of both permanent magnets are varied. The outer flux barrier of the second permanent magnet $\theta_{2,\mathrm{o}}$ correlates to the first slope after the pole intersection. This has to be designed as wide as possible, so that the rotor flux density at the pole intersection follows the sinusoidal function. The last design step of the IPMSM is variation of the remaining flux barrier angles. The objective is to find flux barrier combination, which generates a sufficient amplitude of the flux density fundamental harmonic and simultaneously low THD.

IV. Results

In this section the designed rotor for the alternative machines and the simulation results in no-load, base speed (OP 1) and field weakening area (OP 2) are presented. In no-load operating point machine parameters, back-emf, and cogging torque are evaluated. In OP 1 and OP 2 torque ripple, radial force excitation, copper and iron losses are analyzed. Morever, the air gap flux density of the rotors will be presented.

A. Designed Rotors

In Fig. 4 the geometry of the designed VPMSM rotors are shown. The geometry parameters are listed in Table V. The first rotor (VPMSM 1) is a rotor without the surface modification. The required magnet volume to reach the minimum amplitude of the rotor flux density fundamental harmonics is $7200\,\mathrm{mm}^3$, which is $18.4\,\%$ lower than the reference machine. The THD of the rotor air gap flux density is $27.34\,\%$. To minimized the THD the rotor surface is modified with the method introduced in [12]. To compensate the flux density reduction caused by the taken measures, the permanent magnet width b_{PM} is increased. In Table VI the fundamental harmonics of the rotor flux density and its THD of the rotor with increased magnet width are listed. It is shown that the THD of the rotor flux density is not reduced significantly after $\delta_q/\delta_d = 2.25$. For this reason, the rotor with $\delta_q/\delta_d = 2.25$ is chosen as the second alternative VPMSM (VPMSM 2). The rotor has a magnet volume of $7920\,\mathrm{mm}^3$, which is $10.20\,\%$ lower than the reference machine.

In Fig. 5 the chosen design of the 2-layered IPMSM rotor is shown. The geometry parameter of the rotor are listed in Table VII. The amplitude of the fundamental air gap flux density of the rotor is $0.6\,\mathrm{T}$ with a THD of $14.2\,\%$. The rotor has a similar magnet volume with the VPMSM 2.

In Table VIII the flux densities fundamental harmonic amplitude and the THD of the reference and the alternative rotors are listed. It is shown, that the amplitude of the rotor flux density fundamental harmonic can be reached with lower amount of permanent magnet material. However, the reference rotor, which rotor modification is the combination of the method described in [3] and [4], has a lower THD than the alternative rotors.

In Fig. 6 and Fig. 7 the normalized spatial behavior of the rotor flux densities in the airgap and its harmonics are shown. The flux density curve of the reference rotor is flat in the middle of the pole (d-axis) and follows the sinusoidal shape in the pole intersection. The flat area indicates the position of the uniform surface and the slope the eccentric surface on the rotor, as described in [3]. The smooth transition at the pole intersection is induced by application of the approach described in [4]. With the combination of these methods, all flux density harmonics can be minimized. The

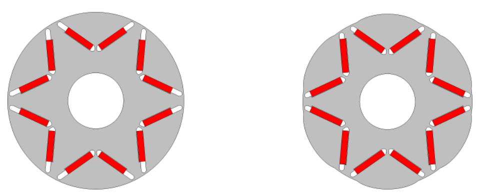

(a) VPMSM 1 (b) VPMSM 2

Fig. 4: The geometry of the designed VPMSM rotors.

TABLE V: Rotor parameter of the designed VPMSM.

		VPMSM	
		Alt. 1	Alt. 2
Air gap ratio δ_q/δ_d	-	1	2.25
Pole pitch factor	-	0.77	
α_{PM}	°	55	
h_{PM}	mm	2	
b_{PM}	mm	10	11
$b_{\mathrm{bridge,mid}}$	mm	0.8	
$b_{\mathrm{bridge,side}}$	mm	0.5	

TABLE VI: Variation of air gap ratio δ_q/δ_d

Air gap ratio δ_q/δ_d	Fundamental Harmonic B_1 / T	THD / %
1	0.68	27.11
1.5	0.65	13.34
1.75	0.66	8.5
2	0.66	5.22
2.25	0.66	3.62
2.5	0.66	3.16
3	0.66	3.14

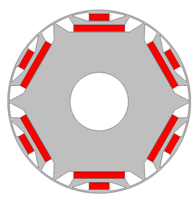

Fig. 5: The geometry of the designed IPMSM rotor.

TABLE VII: Rotor parameter of the designed 2-layered IPMSM.

$h_{\mathrm{PM},1}, h_{\mathrm{PM},2}$	mm	2
$b_{\mathrm{PM},1}/b_{\mathrm{PM},2}$	mm	6 / 16
$\theta_{1,\mathrm{i}}/\theta_{1,\mathrm{o}}$	°	120 / 160
$\theta_{2,\mathrm{i}}/\theta_{2,\mathrm{o}}$	°	120 / 147.5
d_1/d_2	mm	1.5 / 1.25
$b_{\mathrm{barrier},1}/b_{\mathrm{barrier},2}$	mm	7.5 / 19.2

TABLE VIII: The rotor air gap flux densities.

	1-layered IPMSM (ref.)	VPMSM Alt. 1	VPMSM Alt. 2	2-layered IPMSM
Fundamental harmonic B_1 / T	0.6	0.6	0.66	0.6
THD / %	2.95	27.34	3.62	14.2
Magnet volume / mm^3	8820	7200	7920	

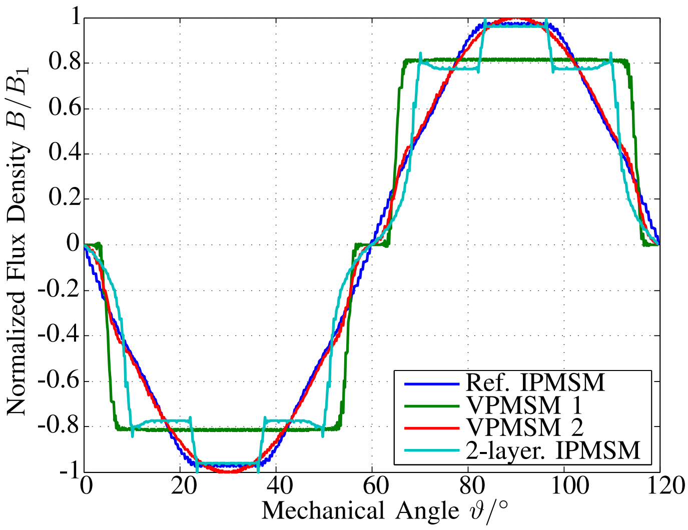

Fig. 6: The air gap flux density of the rotors normalized to the fundamental harmonics.

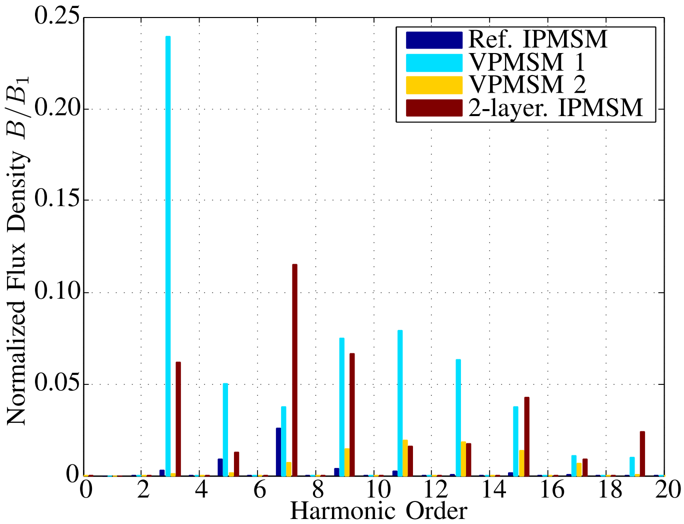

Fig. 7: The harmonics of the air gap flux density of the rotors normalized to the fundamental harmonics.

highest amplitudes of the harmonics are 1 % and 2.6 % of the fundamental harmonic, which is the 5^{th} and 7^{th} harmonics of the flux density respectively.

The effect of rotor surface modification according to [12] can be seen in the flux density behavior of both VPMSMs. Without rotor modification (VPMSM 1), the flux density has a trapezoidal shape on the d-axis with a stepped transition at the pole intersection. Due to the rotor modification (VPMSM 2), the flux density on the d-axis follows a sinusoidal function and has smoother transition on the q-axis. The behavior on the pole intersection has less sinusoidal form when compared to the flux density of the reference machine. The effect of the taken measure can also be seen on the harmonics of the flux density, all of the flux density harmonics of VPMSM 2 are lower than the first VPMSM. Compared to the reference machine, VPMSM 2 has a low normalized amplitude of the 3^{rd}, 5^{th} and 7^{th} harmonics. Starting at 9^{th} harmonics, the normalized amplitude of the harmonics are higher than the ones of the reference machine. It can be concluded, that a rotor modification near d-axis has a dominant effect to the lower harmonics of the flux density characteristic.

The flux density characteristic of the 2-layered IPMSM is different to the 1-layered IPMSM and the VPMSM. Due to the flux barriers, the flux density has a stepped trapezoidal shape. The slopes correlates to the position of the flux barriers and the plateaus to the region on the d-axis and the region between the barriers (between $\theta_{1,\text{o}}$ and $\theta_{2,\text{i}}$). Hence, the outer angle of the second flux barrier $\theta_{2,0}$ has to be wide to create a smooth transition between the pole intersection. If a small angle $\theta_{2,0}$ is chosen, the transition follows the behavior of the VPMSM without surface modification. The flux density curve on the d-axis can be influenced through the combination of permanent magnet widths of the first and second magnet. Due to its stepped form on the d-axis, the 3^{rd} and 5^{th} harmonics of the flux density are minimized. The normalized amplitude of its 7^{th} harmonic is high, when compared to the other rotors.

B. No-Load Simulations

In Table IX the simulation results of the machine in no-load operating point are listed. Due to the similar values of the fundamental harmonic of the flux density, the permanent magnet flux linkage of the rotors are also similar with a deviation of maximum of $\pm 4\,\%$ to their mean value. Hence, the amplitudes of the back-emf fundamental harmonic are also similar. The effects of the rotor modification can be analyzed through examining the relation of the back-emf and inductivity in d- and q-axis with the flux density curves and their harmonics.

In Fig. 8 the normalized back-emf harmonics of each machine are shown. The dominant back-emf of the reference machines are the 5^{th} and 7^{th} harmonics, whose amplitudes are 1.65 % and 0.65 % of the fundamental harmonic respectively. These are related to the dominant harmonic orders of the rotor flux density. Due to larger air gap in the q-axis, the inductivity L_{q} is reduced and the reluctance of the machine is low when compared to a rotor without surface modification. The cogging torque of the reference machine is particularly low at 2.5 mNm.

TABLE IX: The no-load simulation results.

	1-layered IPMSM (ref.)	VPMSM Alt. 1	VPMSM Alt. 2	2-layered IPMSM
PM flux linkage ψ_{F} / mVs	72.9	68.7	73.4	71.5
Inductivity L_{d} / mH	20.5	25.4	22.7	21.1
Inductivity L_{q} / mH	22.5	34.9	25.2	30.6
Saliency ratio $L_{\text{q}}/L_{\text{d}}$	1.1	1.37	1.11	1.45
Back-emf (phase-to-line)				
at $n = 1000\,\text{min}^{-1}$ / V	32.43	30.53	32.65	31.79
Cogging torque / mNm	2.5	19.8	25	82.5

Due to the rotor surface alteration, the back-emf harmonics of VPMSM 2 are generally lower than VPMSM 1. An exception occurs in the 5^{th} harmonics, which is caused by the higher amplitude of the VPMSM 2 rotor flux density on the d-axis. The values of the inductivity L_{d} and L_{q} are reduced due to the form of the air gap. The effect is greater on the q-axis, which reduces the reluctance of VPMSM 2. The cogging torque of VPMSM 2 is slightly higher than VPMSM 1, which is caused by its higher fundamental flux density and its form on the d-axis.

The dominant back-emf harmonic of the 2-layered IPMSM are the 7^{th} harmonic, which is correlated to the harmonics of the rotor flux density. The amplitude of the higher back-emf harmonics of the 2-layered IPMSM, particularly 13^{th}, 17^{th}, 19^{th}, are also higher than the other rotors. Hence, the cogging torque of this machine is also high with 82.5 mNm. Due to its round surface, the 2-layered IPMSM has a similar reluctance behavior to VPMSM 1.

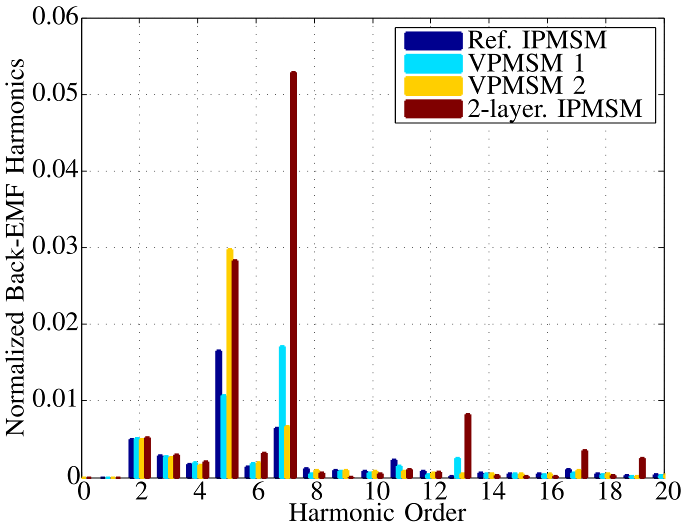

Fig. 8: The harmonics of the no-load back-emf at $n = 1000\,\mathrm{min}^{-1}$ normalized to the fundamental harmonics.

TABLE X: Operating Points of the Alternative Machines

	OP 1			OP 2		
Speed / rpm	610			19520		
Torque / Nm	1.31			0.26		
Output power / W	83.68			531.47		
	VPMSM		2L-IPMSM	VPMSM		2L-IPMSM
Air gap ratio δ_q/δ_d	1	2.25	1	1	2.25	1
Copper losses / W	40.80	38.98	39	37.90	53.43	66.51
Iron losses / W	3.47	3.20	3.14	43.30	33.45	49.10
Efficiency / %	64.80	65.90	65.89	81.90	81.10	77.73
Torque ripple / Nm	0.03	0.04	0.11	0.04	0.02	0.09
Radial force density orders (temporal, spatial) / $\mathrm{kN/m^2}$						
(6, -3)	26.31	20.84	16.20	8.42	4.02	3.00
(6, 6)	11.11	10.91	9.67	6.89	4.78	4.01
(12, -6)	0.70	0.79	0.33	1.26	0.65	0.02
(12, 3)	2.92	1.66	0.32	2.57	1.85	0.48
(18, 0)	0.85	0.48	0.58	0.24	0.06	0.24
Magnet volume / $\mathrm{mm^3}$	7200	7920	7920	7200	7920	7920

C. Machine Operating Points

In Table X the simulation results of the alternative machines in both operating points OP 1 and OP 2 are listed. It is shown, that the efficiencies of the designed machines satisfy the requirements of 62 % and 74 % in the base speed and field weakening operating point respectively. The difference on the copper losses lies on the fundamental harmonic of the rotor flux densities and the saliency of the machines. The VPMSM 2 has a higher fundamental harmonic, but lower saliency than the ones of VPMSM 1 and the 2-layered IPMSM. The difference on the iron losses lies on the amplitudes of the fundamental and the higher harmonics of the rotor flux densities.

In OP 1, VPMSM 2 requires the lowest current density to reach the required torque, regardless its low saliency. This is caused by the amplitude of the rotor flux density fundamental harmonic, which is 10 % higher than the other rotors. The fundamental harmonic of the VPMSM 1 and the 2-layered IPMSM are similar. The higher copper losses of VPMSM 1 are caused by the low saliency, when compared to the saliency of the 2-layered IPMSM. The iron losses of VPMSM 1 are higher than the ones of VPMSM 2 and the 2-layered IPMSM. This is caused by its high THD of the rotor flux density. The high torque ripple of the 2-layered IPMSM is caused by the high 5^{th} and 7^{th} harmonics of the rotor flux density, which is in total 12.8 % of the fundamental harmonic. The radial force excitations, which are correlated to the acoustic radiation, are not relevant in this operating point.

In OP 2, the current density to reach the required torque depends on the field weakening behavior of the machines. Due to the arrangement of the magnets, the 2-layered IPMSM requires a high field weakening current to weaken the permanent magnet flux when compared to the VPMSM. The second permanent magnet of the 2-layered IPMSM induces the first trapezoidal curve of the flux density, which has more influence on the amplitude of the fundamental harmonic. However, the first permanent magnet has to be weakened prior to the second permanent magnet. In case of VPMSM, both magnets have the same position and can be weakened simultaneously. Because of the higher amplitude of the fundamental harmonics, VPMSM 2 requires higher field weakening current than VPMSM 1. The iron losses are dependent on the amplitude of the flux density harmonics. However, the iron losses of the 2-layered IPMSM are higher than VPMSM 1, which is generated by high flux density induced by the flux weakening current. The reason of the high torque ripple of the 2-layered IPMSM is similar to OP 1, which is the high 5^{th} and 7^{th} harmonics of the rotor flux density. Due to the lower THD, the radial force densities of VPMSM 2 are lower than the ones of VPMSM 1. Although the THD is low, these force densities are slightly higher than the ones of the 2-layered IPMSM. To analyze this effect, a space vector convolution according to [18] has to be performed. The origin of the flux density which generates these force excitations can thereby be determined.

V. Conclusions

Three PMSM are designed as an alternative to a reference machine. The machines have lower magnet volume than the reference machine and satisfy the requirements concerning the efficiencies in relevant operating points OP 1 and OP 2. The behavior of the machines in OP 1, except the torque ripple of the 2-layered IPMSM, are similar to each other. In OP 2, VPMSM 2 shows a good balance between high efficiency, low torque ripple and radial force excitation.

A VPMSM without rotor modification has a good agreement between the synchronous and reluctance torque. The rotor requires the lowest magnet volume to reach the minimum amplitude of the rotor flux density fundamental harmonics and has a good $L_\mathrm{q}/L_\mathrm{d}$-ratio. Due to the high THD of the rotor flux density, the rotor has a disadvantage regarding its parasitic effects. The torque ripple, radial force excitations and the iron losses are particularly high. To subdue this effect, the rotor surface is modified, which leads to decrease of the rotor flux density harmonic amplitudes and the reluctance characteristic. As a compensation, the amount of the used permanent magnet material has to be increased. In this case, with 10 % increase on magnet material a machine with similar efficiencies but lower torque ripple and radial force excitations is designed. The increase of the copper losses in field weakening range due to lower saliency evens the decrease ot the iron losses. A 2-layered IPMSM exhibit a high reluctance torque, but low synchronous torque when compared to a VPMSM. The advantage of a 2-layered IPMSM to VPMSM is the possibility to manipulate the form of the rotor flux density without rotor surface modification and the reluctance torque is thereby preserved. However, 2-layered IPMSM has a disadvantage in field weakening range. The permanent magnet near the air gap has to be weakened prior to the second permanent magnet, which increase the required flux weakening current and the iron losses. The torque ripple is also high, when compared to a VPMSM with surface modification. The radial force excitations of both machines are similar to each others.

Concerning the machine characteristics in both operating points, the VPMSM with surface modification is chosen as the most suitable alternative to the reference machine. Further discussion about the machine characteristics in the whole operating area as well as measurement results will be presented in future work.

References

[1] B.E. Donald, D. W. Novotny, T. A. Lipo, "Field weakening in buried permanent magnets AC motor drives", *IEEE Transactions on Industry Applications*, vol. 21, no. 2, pp. 398-407, March-April 1987.

[2] W. Soong nad T. J. E. Miller, "Field weakening performance of brushless synchronous AC motor drives", *IEEE Proceedings-Electric Power Applications*, vol. 141, no. 6, pp. 331-340, November 1994.

[3] K.-Y. Hwang, S.-B. Rhee, B.-Y. Yang, B.-I. Kwon, "Rotor pole design in spoke-type brushless DC Motor by response surface method", *IEEE Transactions on Magnetics*, vol. 43, no. 4, pp. 1833-1836, 2007.

[4] K.-W. Jeon, T.-Y. Lee, Y.-J. Kim, S.-Y. Jung, "Numerical shape design characteristics of torque ripple reduction for interior permanent magnet synchronous motor", *Int. Conf. on Computation in Electromagnetics (CEM)*, London, 2014.

[5] F. Henrotte, M. Felden, M. van der Giet, K. Hameyer, "Electromagnetic force computation with the Eggshell method", *Proc. 14th International Symposium on Numerical Field Calculation in Electrical Engineering (IGTE)*, Graz, 2010.

[6] F. Henrotte, G. Deliege, K. Hameyer, "The eggshell approach for the computationof electromagnetic forces in 2D and 3D", *COMPEL: The International Journal for Computation and Mathematics in Electrical and Electronic Engineering*, Vol. 23, No. 4, pp. 996-1005, 2004.

[7] S. A. Gelfand, *Essentials of Audiology*, Thieme Med. Publishers, 2009.

[8] D. Eggers, S. Steentjes, K. Hameyer, "Advanced Iron-Loss Estimation for Nonlinear Material Behavior", *IEEE Transactions on Magnetics*, Vol. 48, No. 11, pp. 3021-3024, 2012.

[9] S.Steentjes, D. Eggers, M. Lessmann, K. Hameyer, "Iron-loss model for the FE-simulation of electrical machines", *INDUCTICA Technical Conf., CWIEME*, pp. 239-246, Prof. Dr. G. Monkman, Berlin, 2012.

[10] R. De Doncker, D. Pulle, A. Veltmann, *Advanced Electrical Drives: Analysis, Modeling, Control*, Springer, 2010.

[11] A. Wang, Y. Jia, W. L. Soong, "Comparison of five topologies for an interior permanent-magnet machine for a hybrid electric vehicle", *IEEE Transactions on Magnetics*, vol. 47, no. 10, pp. 3606-3609, 2011.

[12] R. Richter, *Elektrische Maschinen: Allgemeine Berechnungselemente*, Birkhäuser, 1951.

[13] C. Andrei et al., "Improved rotor pole geometry of a PMSM for wind turbine applications with multiple high-speed generators", in *2014 International Conference on Optimization of Electrical and Electronic Equipment (OPTIM)*, pp. 450-457, Brasov, 2014.

[14] S. A. Evans, "Salient pole shoe shapes of interior permanent magnet synchronous machines", in *XIX International Conference on Electrical Machines (ICEM)*, pp. 1-6, Rome, 2010.

[15] T. Finken, Fahrzyklusgerechte Auslegung von permanentmagneterregten Synchronmaschinen für Hybrid- und Elektrofahrzeugen, Ph.D. dissertation, Faculty of Electrical Engineering and Information Technology, RWTH Aachen University, Aachen, 2011.

[16] L. Fang, J.-W. Jung, J.-P. Hong, J.-H. Lee, "Study on High-Efficiency Performance in Interior Permanent-Magnet Synchronous Motor With Double-Layer PM Design", *IEEE Transactions on Magnetics*, vol. 44, no. 11, pp. 4393-4396, 2008.

[17] S. Rick, A. K. Putri, D. Franck, K. Hameyer, "Permanent Magnet Synchronous Reluctance Machine - Design guidelines to improve the acoustic behavior", in *XXI International Conference on Electrical Machines (ICEM)*, pp. 1383-1389, Berlin, 2014.

[18] M. van der Giet, R. Rothe, M.H. Gracia, K. Hameyer, "Analysis of noise exciting magnetic force waves by means of numerical simulation and a space vector definition", *18th International Conference on Electrical Machines (ICEM)*, Vilamoura, 2008.

VI. Biographies

Aryanti Kusuma Putri received the M.Sc. degree in electrical engineering from RWTH Aachen University, Germany, in April 2013. She has been working as a research associate at the Institute of Electrical Machines since June 2013. Her research interests include parasitic effects in electrical machines, simulation and design of electrical machines.

Marco Hombitzer received the Dipl.-Ing. degree in electrical engineering from RWTH Aachen University, Germany, in 2010. Since 2010, he has been a researcher at the Institute of Electrical Machines. His research fields include the simulation, the design and performance improvement of electrical machines.

David Franck received the Dipl.-Ing. degree in electrical engineering from RWTH Aachen University, Germany, in March 2008. After that he became of staff (research associate) at the Institute of Electrical Machines. Since 2011 he has been working as chief engineer of the Institute of Electrical Machines. His main field of research is the acoustic behavior of the electrical machines.

Dr. Kay Hameyer received his M.Sc. degree in electrical engineering from the University of Hannover and his Ph.D. degree from the Berlin University of Technology, Germany. After his university studies he worked with the Robert Bosch GmbH in Stuttgart, Germany as a Design Engineer for permanent magnet servo motors and vehicle board net components. Until 2004 Dr. Hameyer was a full Professor for Numerical Field Computations and Electrical Machines with the KU Leuven in Belgium. Since 2004, he is full professor and the director of the Institute of Electrical Machines (IEM) at RWTH Aachen University in Germany. 2006 he was vice dean of the faculty and from 2007 to 2009 he was the dean of the faculty of Electrical Engineering and Information Technology of RWTH Aachen University. His research interests are numerical field computation and optimization, the design and controls of electrical machines, in particular permanent magnet excited machines, induction machines and the design employing the methodology of virtual reality. Since several years Dr. Hameyers work is concerned with the magnetic levitation for drive systems, magnetically excited audible noise in electrical machines and the characterization of ferro-magnetic materials. Dr. Hameyer is author of more than 250 journal publications, more than 500 international conference publications and author of 4 books. Dr. Hameyer is a member of VDE, IEEE senior member, fellow of the IET.